The Different Role of Cavitation on Rotordynamic Whirl Forces in Axial Inducers and Centrifugal Impellers

Luca d'Agostino[1]

[1] Dipartimento di Ingegneria Aerospaziale, Università di Pisa, Pisa, Italy

Abstract. The linearized dynamics of the flow in cavitating axial helical inducers and centrifugal turbopomp impellers is investigated with the purpose of illustrating the impact of the dynamic response of cavitation on the rotordynamic forces exerted by the fluid on the rotors of whirling turbopumps. The flow in the impellers is modeled as a fully-guided, incompressible and inviscid liquid. Cavitation is included through the boundary conditions on the suction sides of the blades, where it is assumed to occur uniformly in a small layer of given thickness and complex acoustic admittance, whose value depends on the void fraction of the vapor phase and the phase-shift damping coefficient used to account for the energy dissipation. Constant boundary conditions for the total pressure are imposed at the inlet and outlet sections of the impeller blade channels. The unsteady governing equations are written in rotating "body fitted" orthogonal coordinates, linearized for small-amplitude whirl perturbations of the mean steady flow, and solved by modal decomposition. In helical turbopump inducers the whirl excitation and the boundary conditions generate internal flow resonances in the blade channels, leading to a complex dependence of the lateral rotordynamic fluid forces on the whirl speed, the dynamic properties of the cavitation region and the flow coefficient of the machine. Multiple subsynchronous and supersynchronous resonances are predicted. At higher levels of cavitation the amplitudes of these resonances decrease and their frequencies approach the rotational speed (synchronous conditions). On the other hand, application of the same approach indicates that no such resonances occur in whirling and cavitating centrifugal impellers and that the rotordynamic fluid forces are almost insensitive to cavitation, consistently with the available experimental evidence. Comparison with the scant data from the literature indicates that the present theory correctly captures the observed features and parametric trends of rotordynamic forces on whirling and cavitating turbopump impellers. Hence there are reasons to believe that it can usefully contribute to shed some light on the main physical phenomena involved and provide practical indications on their dependence on the relevant flow conditions and parameters.

1 Introduction

Local flow phenomena, like tip leakage, capable of interfering with the blade loading are known to be the dominant source of rotordynamic whirl forces in compressible flow machines (Thomas, 1958; Alford, 1958; Martinez-Sanchez et al., 1995; Martinez-Sanchez and Song, 1997a, 1997b).

Previous research efforts in turbopumps mainly focused on the origin and analysis of rotordynamic impeller forces under noncavitating conditions (Chamieh et al., 1985; Jery, 1985; Jery et al., 1987; Shoji and Ohashi, 1987; Ohashi & Shoji 1987; Adkins and Brennen, 1988; Arndt et al., 1989, 1990; Tsujimoto et al., 1997; Uy and Brennen, 1999; Baskharone, 1999; Hiwata and Tsujimoto, 2002). However, it is widely recognized that cavitation in turbopumps can promote the onset of dangerous self-sustained whirl instabilities (Rosenmann, 1965) and substantially modify the behavior of fluid-induced rotordynamic forces on helical inducers (Arndt and Franz, 1986; Brennen, 1994; Bhattacharyya, 1994), where the large-scale dynamic response of the entire flow to the impeller whirl motion seems to play a significant role (d'Auria, d'Agostino and Brennen, 1995; d'Agostino and d'Auria, 1997; d'Agostino, d'Auria and Brennen, 1998; d'Agostino and Venturini, 2002, 2003). Because of their greater complexity, rotordynamic fluid forces in whirling and cavitating turbopump impellers have so far received comparatively less attention in the open literature and a satisfactory understanding of their behavior is still lacking.

The available experimental evidence indicates that cavitation affects the added mass of the rotor and significantly reduces the magnitude of the rotordynamic fluid forces on helical inducers. It is worth noting that the consequent increase of the critical speeds is especially dangerous in supercritical machines, commonly used in liquid propellant rocket feed systems. A second major effect of cavitation in helical inducers is the introduction of a complex oscillatory dependence of the rotordynamic fluid forces on the whirl frequency. This finding seems to indicate the possible occurrence of resonance phenomena in the compressible cavitating flow inside the inducer blade channels under the excitation imposed by the eccentric motion of the rotor. Earlier theoretical analyses aimed at investigating this hypothesis have addressed the case of infinitely-long whirling helical inducers with uniformly distributed traveling bubble cavitation (d'Auria et al., 1995; d'Agostino and d'Auria, 1997; d'Agostino, d'Auria and Brennen 1998). The results confirmed the presence of internal flow resonances and indicate that bubble dynamic effects do not play a major role, except, perhaps, at extremely high whirl speeds. They also suggest that the assumptions of uniformly-distributed bubbly cavitation and infinitely long inducers may contribute to explain the discrepancies between theoretical predictions and experimental data. On the other hand, no resonant phenomena seem to occur in radial impellers, where the limited available evidence indicates that cavitation only has a marginal effect on the rotordynamic whirl forces (Franz et al., 1989).

Following up on this work, we now investigate the dynamics of the unsteady flow in whirling helical inducers and radial impellers with attached blade cavitation, in order to gain some better understanding of the fundamental reasons for the different behavior of rotordynamic fluid forces in this two kinds of turbomachines. Upon introduction of suitable simplifying approximations, the flow is linearized for small-amplitude whirl motions of the rotor and solved by modal expansion. In spite of the simplifications introduced in order to obtain an efficient closed form solution, comparison with the available experimental data indicates that the proposed analyses correctly predict the main observed features and differences of the rotordynamic fluid forces in whirling and cavitating inducers and radial impellers, thus providing useful practical indications and fundamental understanding of their dependence on the relevant flow conditions and parameters.

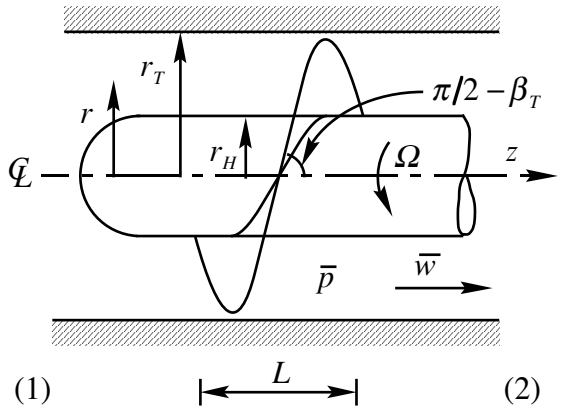

Figure 1. Schematic of the flow configuration and inducer geometry.

2 Linearized Dynamics of the Cavitating Flow in a Whirling Inducer

We first examine the dynamics of an incompressible, inviscid liquid of velocity $\boldsymbol{u}$, pressure p, and density ρ_L in a helical inducer rotating with velocity $\boldsymbol{\Omega}$ and whirling on a circular orbit of small eccentricity ε at angular speed ω. A number of simplifications are introduced in order to reduce the problem to a form admitting an analytical solution. As illustrated in Figure 1, a simple helical inducer is considered, with N_B radial blades, zero blade thickness, axial length L, hub

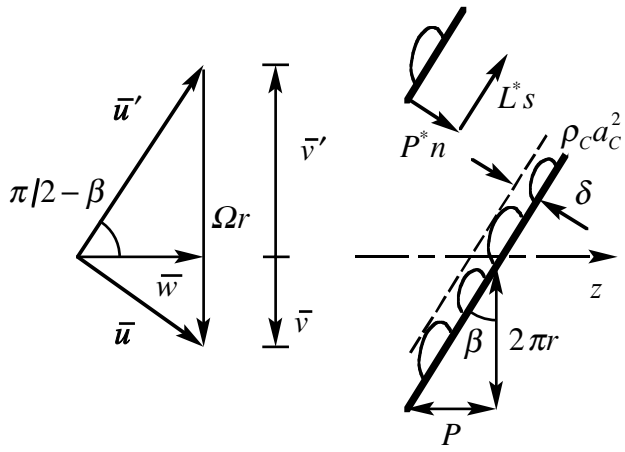

Figure 2. Schematic of the thin layer of attached cavitation pockets on the suction sides of the inducer blades.

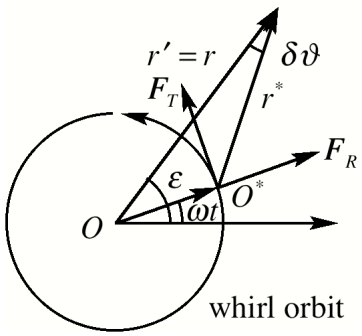

Figure 3. Schematic of whirl motion, coordinates and rotordynamic forces.

radius r_H, tip radius r_T, tip blade angle β_T, and constant pitch:

$$P = 2\pi r_T \tan\beta_T = 2\pi r^* \tan\beta$$

The flow is fully wetted everywhere except on the suction sides of the blades, where attached cavitation occurs. The mean flow velocity $\bar{\boldsymbol{u}}$ in the blade channels is specified by the flow coefficient $\phi = \bar{w}/\Omega r_T$, assuming fully-guided forced-vortex flow with zero radial velocity $\bar{u}$, uniform axial velocity $\bar{w}$, and angular velocity $\Omega_F = \bar{v}/r = \Omega\left(1-\phi\cot\beta_T\right)$. With reference to Figure 2, cavitation is thought to occur on the suction sides of the blades in the form of slowly-moving attached pockets uniformly distributed in a thin layer of given thickness $\delta << P$ and damped acoustic admittance $\rho_C a_C^2\left(1+i\zeta\right)$, where ζ is a nondimensional damping coefficient. The static pressure p_C in the cavitating layer is taken equal to the total pressure p_t of the surrounding liquid, assuming that the flow slows down without losses in the low velocity region between the cavities.

We define stationary cylindrical coordinates r, ϑ, z with center in O on the axis of the stator, rotating cylindrical coordinates r', ϑ', z' spinning at the rotor speed with center in the same point O, and rotating and whirling cylindrical coordinates r^*, ϑ^*, z^* fixed in the inducer and with center in O^* on its geometric axis, as shown in Figure 3. Then the equations of the blade surfaces are:

$$B = \vartheta^* + \frac{2\pi}{P} z^* - \vartheta_j = 0$$

where $\vartheta_j = 2\pi\left(j-1\right)/N_B$ is the angular location of the j-th blade, with $j = 1, 2, ..., N_B$. The flow velocities in the stationary and rotating frames are related by $\boldsymbol{u} = \boldsymbol{u}' + \boldsymbol{\Omega}\times\boldsymbol{r}$ and, to the first order in the eccentricity:

$$r^* = r - \varepsilon\cos\left(\vartheta - \omega t\right) = r' - \varepsilon\cos\left(\vartheta' - \omega' t\right)$$

$$\vartheta^* = \vartheta - \Omega t + \frac{\varepsilon}{r}\sin\left(\vartheta - \omega t\right) = \vartheta' + \frac{\varepsilon}{r}\sin\left(\vartheta' - \omega' t\right)$$

$$z^* = z' = z$$

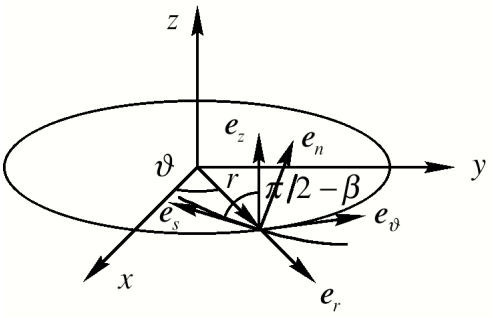

Figure 4. Schematic of the transformation from the cylindrical coordinates r,ϑ,z to the orthogonal helical coordinates r,n,s .

where $\omega' = \omega - \Omega$.

Neglecting Coriolis forces, the perturbation velocity $\tilde{\boldsymbol{u}}$ in the frame moving with the mean flow at axial velocity $\bar{w}$ and angular speed Ω_F is irrotational ($\tilde{\boldsymbol{u}} = \nabla\tilde{\varphi}$) because it originates from a resting flow with conservative centrifugal forces. Therefore, in the rotating frame the flow velocity is $\boldsymbol{u}' = \left(\boldsymbol{\Omega}_F - \boldsymbol{\Omega}\right)\times\boldsymbol{r} + \bar{\boldsymbol{w}} + \nabla\tilde{\varphi}$ and the Bernoulli's equation writes:

$$\int \frac{\partial'\boldsymbol{u}'}{\partial t}\cdot d\boldsymbol{x} + \frac{1}{2}\boldsymbol{u}'\cdot\boldsymbol{u}' - \frac{1}{2}\Omega^2\boldsymbol{r}\cdot\boldsymbol{r} + \frac{p}{\rho_L} = \int \boldsymbol{u}'\times\left(\nabla\times\boldsymbol{u}'\right)\cdot d\boldsymbol{x}$$

where $\nabla\times\boldsymbol{u}' = 2\left(\boldsymbol{\Omega}_F - \boldsymbol{\Omega}\right)$. Evaluating this equation between the generic point and the corresponding unperturbed conditions on a vorticity line parallel to the inducer axis, the linearized governing equations for the flow perturbations (tildes) in the rotating frame are:

$$\nabla^2\tilde{\varphi} = 0 \qquad \text{and} \qquad \frac{\partial'\tilde{\varphi}}{\partial t} + \bar{\boldsymbol{u}}'\cdot\nabla\tilde{\varphi} + \frac{\tilde{p}}{\rho_L} = 0$$

These equations must be complemented with the appropriate boundary conditions. Here, the flow velocity must satisfy the kinematic conditions $DB/Dt = 0$ on the hub, blade and casing surfaces of equations $B\left(\boldsymbol{x},t\right) = 0$ in the relevant coordinates. In addition, the total pressure is assumed constant on the inlet and outlet sections of the inducer.

In order to simplify the boundary conditions, let introduce orthogonal helical coordinates r,n,s of unit vectors $\boldsymbol{e}_r$, $\boldsymbol{e}_n$, $\boldsymbol{e}_s$ as shown in Figure 4 with:

$$n = \left(\vartheta - \vartheta_j\right)\frac{N_B}{2\pi} + z\frac{N_B}{P}$$

$$s = z\frac{\sin^2\beta}{P} - \left(\vartheta - \vartheta_j\right)\frac{\cos^2\beta}{2\pi}$$

Here, for convenience, n is normalized with the channel width $P^* = \left(P/N_B\right)\cos\beta$ and s with the blade length $L^* = P/\sin\beta$ at the radius corresponding to the angle β . The rotating and body-fixed orthogonal helical coordinates r',n',s' and r^*,n^*,s^* are similarly defined in terms of r',ϑ',z' and r^*,ϑ^*,z^* . Then, the equations of the hub, blade pressure sides, blade suction sides and casing surfaces are:

$$B = r^* - r_H = 0$$

$$B = n^* = 0$$

$$B = n^* - 1 + \delta / P^* = 0$$

$$B = r - r_T = 0$$

where $\delta = \delta(t)$. From the continuity equation for the layer $\rho_C \delta \equiv \text{constant}$, the definition of $a_C^2 = dp_t / d\rho_C$ and the Bernoulli's equation $\tilde{p}_t / \rho_L = -\partial\tilde{\varphi}/\partial t$ it follows that:

$$\frac{d\delta}{dt} = \frac{\rho_L \delta}{\rho_C a_C^2} \frac{\partial^2 \tilde{\varphi}}{\partial t^2}$$

With these results, expressing $\nabla^2 \tilde{\varphi} = 0$ and $\partial B/\partial t + \boldsymbol{u}' \cdot \nabla B = 0$ in the rotating helical coordinates r', n', s':

$$\frac{\partial^2 \tilde{\varphi}}{\partial r'^2} + \frac{1}{r'} \frac{\partial \tilde{\varphi}}{\partial r'} + \frac{N_B^2}{P^2 \cos^2 \beta} \frac{\partial^2 \tilde{\varphi}}{\partial n'^2} + \frac{\cos^2 \beta}{4\pi^2 r'^2} \frac{\partial^2 \tilde{\varphi}}{\partial s'^2} = 0$$

and the linearized boundary conditions are found to be:

$$\frac{\partial \tilde{\varphi}}{\partial r'} = 0 \quad \text{on} \quad r' = r_T$$

$$\frac{\partial \tilde{\varphi}}{\partial r'} = \varepsilon(\omega - \Omega_F) \sin H \quad \text{on} \quad r' = r_H$$

$$\frac{\partial \tilde{\varphi}}{\partial n'} = \frac{\varepsilon(\omega - \Omega_F) P^2 \cos^2 \beta}{2\pi r' N_B} \cos H \quad \text{on} \quad n' = 0$$

$$\frac{\partial \tilde{\varphi}}{\partial n'} + K_C \frac{\partial^2 \tilde{\varphi}}{\partial t^2} = \frac{\varepsilon(\omega - \Omega_F) P^2 \cos^2 \beta}{2\pi r' N_B} \cos H \quad \text{on} \quad n' = 1$$

$$\frac{\partial \tilde{\varphi}}{\partial t} = 0 \quad \text{on} \quad s' = s_i' = -\frac{\cos^2 \beta}{2N_B}, \; s_i' + N_R$$

where:

$$H = \frac{2\pi}{N_B} n' \sin^2 \beta - 2\pi s' + \vartheta_j - \omega' t$$

$$K_C = \frac{\rho_L \delta P^*}{\rho_C a_C^2 (1 + i\zeta)}$$

is a parameter describing the behavior of the cavitating layer, and N_R is the number of revolutions of the blade channels about the inducer axis.

With the above boundary conditions the Laplace equation for $\tilde{\varphi} = \text{Re}\{\hat{\varphi}\}$ yields a well-posed boundary value problem for the complex velocity potential $\hat{\varphi}$. If the variable blade angle β is approximated by a constant value β_M at some suitable mean radius r_M, the separable solution (Lebedev, 1965) in the blade channels $0 \le n' \le 1$ is:

$$\hat{\varphi} = \hat{\varphi}_H + \hat{\varphi}_B$$

where:

$$\hat{\varphi}_H = \sum_{k=1}^{+\infty}\sum_{m=1}^{+\infty} R_{km}\left(r'\right) N_k\left(n'\right) S_m\left(s'\right) e^{-i\omega' t}$$

$$\hat{\varphi}_B = \sum_{l=1}^{+\infty}\sum_{m=1}^{+\infty} R_{lm}\left(r'\right) N_{lm}\left(n'\right) S_m\left(s'\right) e^{-i\omega' t}$$

are the solutions corresponding to the hub and blade excitation. In the expression of $\hat{\varphi}_H$:

$$R_{km}\left(r'\right) = I_{km}\frac{K'_{q_m}\left(\lambda_k^* r_T\right) I_{q_m}\left(\lambda_k^* r'\right) - I'_{q_m}\left(\lambda_k^* r_T\right) K_{q_m}\left(\lambda_k^* r'\right)}{I'_{q_m}\left(\lambda_k^* r_H\right) K'_{q_m}\left(\lambda_k^* r_T\right) - K'_{q_m}\left(\lambda_k^* r_H\right) I'_{q_m}\left(\lambda_k^* r_T\right)}$$

$$N_k\left(n'\right) = \cos\left(n'\sqrt{-\nu_k^2}\right)$$

are the coupled modal solutions corresponding to the hub excitation, where:

$$\lambda_k^* = \frac{N_B}{P\cos\beta_M}\sqrt{-\nu_k^2}$$

and $\sqrt{-\nu_k^2}$ are the (complex) principal roots of the equation:

$$\sqrt{-\nu^2}\,\sin\sqrt{-\nu^2} = -K_C\omega'^2\cos\sqrt{-\nu^2}$$

Similarly, in the expression of $\hat{\varphi}_B$:

$$R_{lm}\left(r'\right) = Y'_{q_m}\left(\lambda_{lm} r_H\right) J_{q_m}\left(\lambda_{lm} r'\right) - J'_{q_m}\left(\lambda_{lm} r_H\right) Y_{q_m}\left(\lambda_{lm} r'\right)$$

$$N_{lm}\left(n'\right) = \frac{I\left(1\right)\cosh\left(\nu_{lm} n'\right) - I\left(0\right)\cosh\left[\nu_{lm}\left(n'-1\right)\right]}{\nu_{lm}\sinh\nu_{lm} - K_C\omega'^2\cosh\nu_{lm}} +$$

$$-\frac{I\left(0\right)K_C\omega'^2}{\nu_{lm}\sinh\nu_{lm} - K_C\omega'^2\cosh\nu_{lm}}\frac{\sinh\left[\nu_{lm}\left(n'-1\right)\right]}{\nu_{lm}}$$

are the coupled modal solutions corresponding to the blade excitation, where λ_{lm} are the (positive) roots of the equation:

$$J'_{q_m}\left(\lambda r_H\right) Y'_{q_m}\left(\lambda r_T\right) - Y'_{q_m}\left(\lambda r_H\right) J'_{q_m}\left(\lambda r_T\right) = 0$$

$$\nu_{lm} = \lambda_{lm}\frac{P\cos\beta_M}{N_B}$$

and:

$$I\left(n'\right) = \frac{\varepsilon\left(\omega - \Omega_F\right) P^2\cos^2\beta_M}{\pi N_B N_R} e^{i\left[\left(2\pi/N_B\right)n'\sin^2\beta_M + \vartheta_j\right]} \times$$

$$\times\frac{\int_{r_H}^{r_T} R_{lm}\left(r'\right) dr'}{\int_{r_H}^{r_T} R_{lm}^2\left(r'\right) r'\, dr'}\int_{s'_i}^{s'_i + N_R} e^{-i2\pi s'} S_m\left(s'\right) ds'$$

Finally, in the both of the expressions of $\hat{\varphi}_H$ and $\hat{\varphi}_B$:

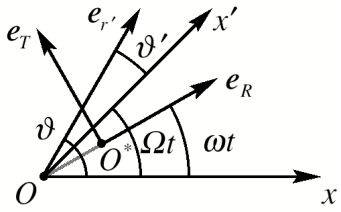

Figure 5. Schematic of the transformation form the rotating frame $O,\boldsymbol{e}_{r'},\boldsymbol{e}_{\vartheta'},\boldsymbol{e}_{z'}$ to the whirling frame $O^*,\boldsymbol{e}_R,\boldsymbol{e}_T,\boldsymbol{e}_z$.

$$q_m = \frac{m}{2N_R}\cos\beta_M \qquad \text{and} \qquad S_m\left(s'\right) = \sin\frac{m\pi\left(s'-s_i'\right)}{N_R}$$

The instantaneous fluid force on the inducer is:

$$\tilde{\boldsymbol{F}} = -\oint_{S_H\cup S_B} p\left(\boldsymbol{x}'\big|_{\varepsilon\neq 0},t\right)d\boldsymbol{S}$$

where the pressure:

$$p = \bar{p} - \rho_L\left(\frac{\partial\tilde{\varphi}}{\partial t} - \frac{\Omega_F-\Omega}{2\pi}\frac{\partial\tilde{\varphi}}{\partial s'}\right)$$

is evaluated for $\varepsilon\neq 0$ at the perturbed position of the hub and blade surfaces S_H and S_B. Thus, expanding to the first order in the eccentricity and noting that the mean pressure $\bar{p}\left(r'\big|_{\varepsilon=0},t\right)$ makes no net contribution to the force on the inducer in its centered position, the following expression for the fluid force on the inducer is obtained:

$$\tilde{\boldsymbol{F}} \cong -\oint_{S_H\cup S_B}\left[\left.\frac{\partial\bar{p}}{\partial r'}\right|_{\varepsilon=0}\left(r'\big|_{\varepsilon\neq 0} - r'\big|_{\varepsilon=0}\right) + \tilde{p}\left(\boldsymbol{x}'\big|_{\varepsilon=0},t\right)\right]d\boldsymbol{S}$$

Here the first term is the buoyancy force on the displaced inducer due to the radial gradient of the mean pressure:

$$\frac{d\bar{p}}{dr'} = \rho_L\Omega^2 r'\left(1-\phi^2\cot^2\beta_T\right)$$

and the second term is the force due to the pressure perturbations generated by the eccentric motion. The components of the instantaneous rotordynamic force are therefore obtained by integrating the projections of the elementary pressure forces along the axes of the whirling frame of center in O^* and unit vectors $\boldsymbol{e}_R$, $\boldsymbol{e}_T$, $\boldsymbol{e}_z$, as shown in Figure 5. Finally, further integration over a period $2\pi/\omega'$ yields the time-averaged rotordynamic force $\bar{\boldsymbol{F}}$ on the inducer.

The entire flow has therefore been determined in terms of the material properties of the two phases, the geometry of the inducer, the nature of the excitation, and the assigned quantities ϕ, δ, ρ_C, a_C and ζ.

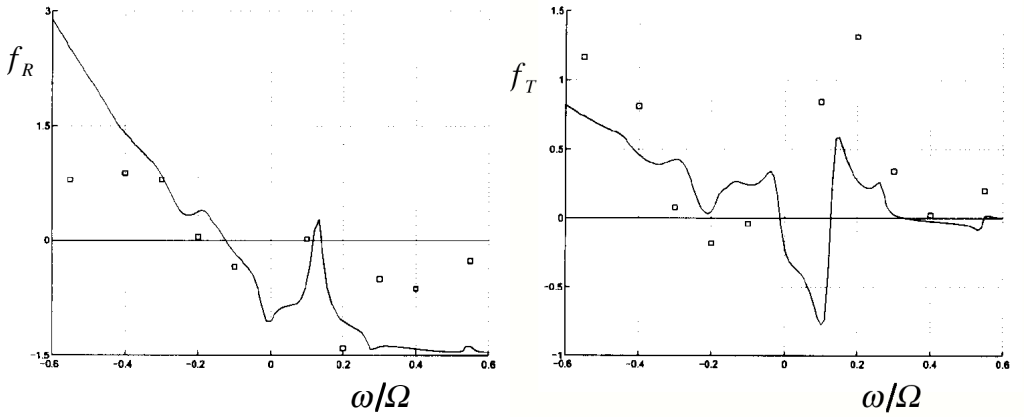

Figure 6. Nondimensional radial rotordynamic force f_R (left) and tangential rotordynamic force f_T (right) on the test inducer as functions of the ratio ω/Ω of the whirl and rotational speeds. The experimental values (circles) obtained by Bhattacharyya, 1994, under developed cavitation conditions at $\phi_1 = 0.049$ and $\sigma_1 = 0.106$ are compared with the model predictions (solid line) for $\phi = \phi_1 \big/ \left(1 - r_H^2 / r_T^2\right) = 0.0583$, $\mathrm{Re}\left\{K_C \Omega^2\right\} = 2.5$, $\zeta = 0.045$ and $N_R = 0.285$.

3 Rotordynamic Forces on Whirling and Cavitating Axial Inducers

The rotordynamic fluid forces predicted by the present model will be compared with the data measured by Bhattacharyya (1994) on a three-bladed helical inducer with $r_T = 5.06$ cm, $r_H / r_T = 0.4$, $\beta_T = 9°$, $L = 2.43$ cm, $\varepsilon = 0.254$ mm. The data refer to operation in water at room temperature, rotational speed $\Omega = 3{,}000$ rpm, variable whirl speed, and several values of the inlet flow coefficient $\phi_1 = \dot{Q} \big/ A_1 \Omega r_T$ (not corrected for hub blockage) and cavitation number $\sigma_1 = \left(p_1 - p_V\right) \big/ \tfrac{1}{2} \rho_L \Omega^2 r_T^2$.

Figures 6 shows some typical experimental results for the nondimensional rotordynamic force $\tilde{\boldsymbol{f}} = \bar{\boldsymbol{F}} \big/ \pi \varepsilon^2 P \rho_L \Omega^2 r_T$ on the sample inducer tested under developed cavitation at $\phi_1 = 0.049$ and $\sigma_1 = 0.106$. Notice that the radial and tangential force components do not vary quadratically with the normalized whirl speed ω/Ω, and that their behavior is characterized by multiple zero crossings. The radial force (left) is essentially positive (destabilizing) for $\omega/\Omega < -0.2$, oscillates above and below zero for $-0.2 < \omega/\Omega < 0.3$, and remains essentially negative (stabilizing) for $\omega/\Omega > 0.3$. Similar behavior was observed for other cavitation numbers (Bhattacharyya, 1994). The tangential force (right) is positive over most of the sampled frequencies, but also exhibits rapid oscillations near the origin. In all of the experiments of Bhattacharyya a peculiar feature of the tangential force is the occurrence of a sharp positive (destabilizing) peak at $\omega/\Omega \cong 0.2$, whose intensity increases at higher cavitation numbers and lower flow coefficients.

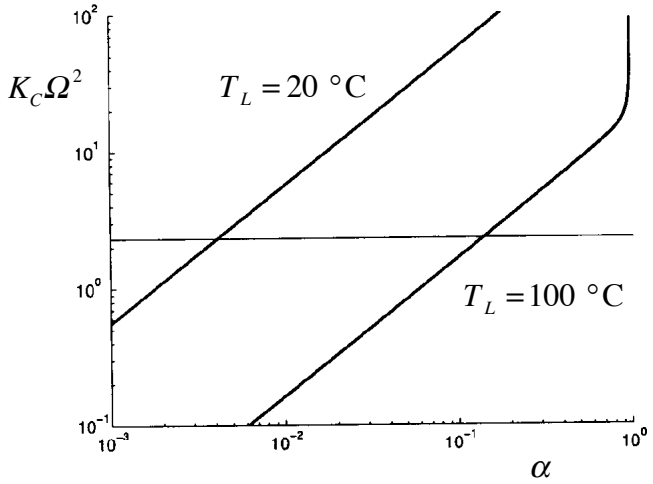

Figure 7. Nondimensional cavitation parameter $K_C\Omega^2$ as a function of the void fraction in the cavitating layer for undamped operation in water at $T_L = 20$ °C ($\delta_T / R = 0.3$, $\delta / P^* = 3\%$) and $T_L = 100$ °C ($\delta_T / R = 1$, $\delta / P^* = 10\%$).

Figures 6 also shows the rotordynamic forces predicted by the present model (continuous line) assuming $\mathrm{Re}\left\{K_C\Omega^2\right\} = 2.5$ for the real part of the cavitation parameter and $\zeta = 0.045$ for the nondimensional damping coefficient. An effective value of the nondimensional blade channel length, $N_R = 0.285$, intermediate between the geometric length of the blades and their actual overlap, has been used in the computations in order to empirically compensate for the errors introduced by the formulation in orthogonal helical coordinates. In addition, the pressure gradient of the mean flow has been evaluated for a decreased value of the swirl speed Ω_F in order to account for the gradual rotational acceleration of the flow entering the inducer. Comparison with the experimental data shows that, in spite of its approximate nature, the present theory correctly captures the observed magnitude of the rotordynamic forces and the typical features of their whirl frequency spectrum, including their stabilizing or destabilizing effects on the eccentric motion of the inducer.

The complex dependence of the lateral rotordynamic fluid forces on the whirl speed is due to the occurrence of internal resonances of the cavitating flow in the blade channels under the excitation generated by the whirl motion of the inducer. Given the functional dependence of the solution, it appears that the system has an infinite set of (generally complex) critical whirl speeds:

$$\omega'_{lm} = \omega_{lm} - \Omega = \pm\sqrt{\frac{\nu_{lm}\tanh\nu_{lm}}{K_C}}$$

symmetrically located above and below the rotational speed Ω (synchronous conditions). The critical speeds are seen to depend on the mode numbers of the flow perturbations and the parameter K_C used to characterize the occurrence of cavitation on the suction sides of the blades. The

extent of cavitation increases when the value of this parameter is varied from zero, corresponding to fully-wetted flow conditions, to larger and larger values. In the special case of vanishing cavitation damping ($\zeta \to 0$), K_C tends to a real value and the boundary value problem for $\hat{\varphi}$ to become self-adjoint, with real eigenvalues λ^2 and ν^2. In the presence of damping, the series for $\hat{\varphi}$ converge rapidly even for low subcritical values of $\zeta << 1$, and only the first few modes are needed in the computations. For these modes the eigenvalues are of order unity or slightly larger. Since cavitating flows are inherently dissipative, it follows that the critical whirl speeds of practical importance tend to concentrate in two small ranges just above and below synchronous conditions as soon as the intensity of cavitation is sufficient for raising the real part of $K_C\Omega^2$ well above unity.

The relation of K_C to the extent of cavitation can be investigated with the help of a suitable flow model. Here we make use of the classical quasi-homogeneous isenthalpic cavitation model with thermal effects described by Brennen (1995) and modified by Rapposelli and d'Agostino (2001) to account for the concentration of active nuclei. The behavior of the real part of $K_C\Omega^2$ with the local void fraction α is illustrated in Figure 7 for water at room and boiling temperature. The results depend parametrically on the blade channel blockage δ/P^* and the ratio δ_T/R between the thermal boundary layer thickness surrounding a spherical cavity and the radius of the cavity itself. The parameter δ_T/R is nearly constant during the thermally controlled growth of cavitating bubbles and its value can be estimated as a function of the flow conditions, the thermophysical properties of the two phases, and the concentration of active cavitation nuclei (Rapposelli and d'Agostino, 2001). Here the choice of a higher blockage δ/P^* at the boiling temperature reflects the greater penetration of cavitation in the liquid at elevated temperatures. From Figure 8 it appears that the value $\mathrm{Re}\left\{K_C\Omega^2\right\} = 2.5$ previously used for the prediction of the rotordynamic forces would correspond to void fractions ranging from $4 \cdot 10^{-2}$ at room temperature to 10^{-1} at boiling conditions. The average separation between bubbles would then be on the order of 2 to 3 diameters, not unrealistic mean values for typical cavitation on inducer blades.

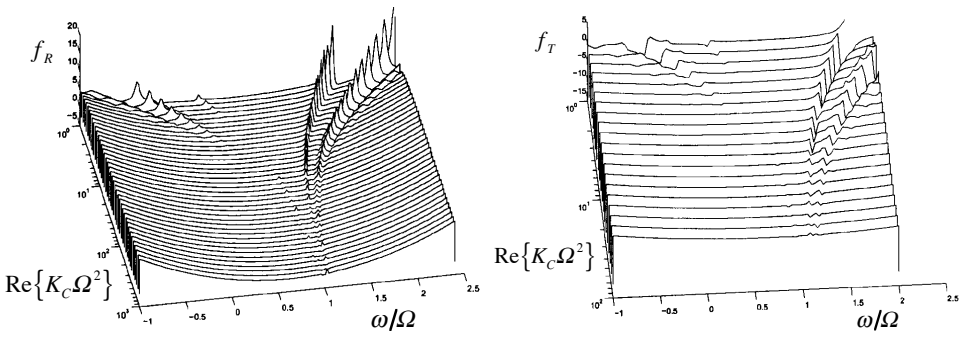

Figure 8. Waterfall plots of the nondimensional radial rotordynamic force f_R (left) and tangential rotordynamic force f_T (right) on the test inducer functions of the ratio ω/Ω of the whirl and rotational speeds and the real part of the nondimensional cavitation parameter, $K_C\Omega^2$. The flow coefficient is $\phi = 0.0583$, the nondimensional damping coefficient is $\zeta = 0.045$ and the effective length of the blade channels is $N_R = 0.285$.

The influence of the cavitation parameter on the solution is illustrated by the waterfall plots of Figure 8. The figure clearly shows that the degree of cavitation has a major impact in locating the critical speeds and determining the magnitude of the rotordynamic forces as functions of the whirl speed. Two sets of subsynchronous and supersynchronous resonances are predicted. At higher values of the cavitation parameter the amplitudes of the resonances decrease, as their frequencies approach synchronous conditions. At low values of $\mathrm{Re}\left\{K_C \Omega^2\right\} << 1$ the void fraction is likely to violate the condition:

$$\left(\alpha\delta\right)_{\min} \approx \varepsilon \sin\beta_M$$

for the survival of the cavitating layer during a complete oscillation cycle of the whirl motion. With typical choices of the relevant quantities, the minimum void fraction is estimated to be $\alpha_{\min} \cong 10^{-2} \div 10^{-1}$. Hence, using the results of Figure 7, the physically significant solutions of the present theory are restricted to minimum values of the cavitation parameter:

$$\mathrm{Re}\left\{K_C \Omega^2\right\}_{\min} \approx 1 \text{ to } 10$$

corresponding to room temperature and boiling conditions, respectively. In this range Figure 8 indicates the presence of two relatively weak subsynchronous critical speeds near $\omega/\Omega \approx 0.5$, and a second couple of considerably more intense supersynchronous critical speeds in the vicinity of $\omega/\Omega \approx 1.5$. The spectral locations of these critical speeds evocatively overlap with the reported ranges of free-whirl instabilities in cavitating turbopumps.

As a final comment, comparison of the data reported in Figure 6 with the results of Figure 8 indicates that the scant experimental information currently available on the behavior of rotordynamic forces in cavitating turbopumps only covers a limited portion of the frequency spectrum, and probably not the most significant one in connection with the onset of cavitation-induced whirl instabilities.

4 Linearized Dynamics of the Cavitating Flow in a Whirling Centrifugal Impeller

With a similar approach, we next examine the dynamics of an incompressible, inviscid liquid of velocity $\boldsymbol{u}$, pressure p, and density ρ_L in a centrifugal pump impeller rotating with velocity Ω and whirling on a circular orbit of small eccentricity ε at angular speed ω. A number of idealizations are introduced in order to obtain an analytical solution. Figure 9 (left) illustrates the simple centrifugal pump considered, with N_B logarithmic-spiral blades of equation $r\,d\vartheta/r = -\tan\beta$, zero blade thickness, axial length b, hub radius r_H, tip radius r_T, blade angle β.

Also in this case the flow is fully wetted everywhere except on the suction sides of the blades, where attached cavitation occurs. The mean flow velocity $\bar{\boldsymbol{u}}$ in the blade channels (on the right in Fig. 9) is specified by the flow coefficient $\phi = \bar{u}_T / \Omega r_T$, assuming fully-guided forced-vortex flow with zero axial velocity $\bar{w}$, radial velocity $\bar{u} = r_T \bar{u}_T / r$, and tangential velocity:

$$\bar{v}^2 = \Omega^2\phi^2\left(r_T^4/r^2\right)\tan^2\beta + \Omega^2 r^2 - 2\Omega^2 r_T^2 \phi \tan\beta$$

Also in this case cavitation is thought to occur on the suction sides of the blades in a thin layer of given variable thickness δ (constant coordinate n, see below) and acoustic admittance $\rho_C a_C^2$. For simplicity, it is also assumed that the static pressure p_C in the cavitating layer is nearly equal to the total pressure p_t of the surrounding liquid.

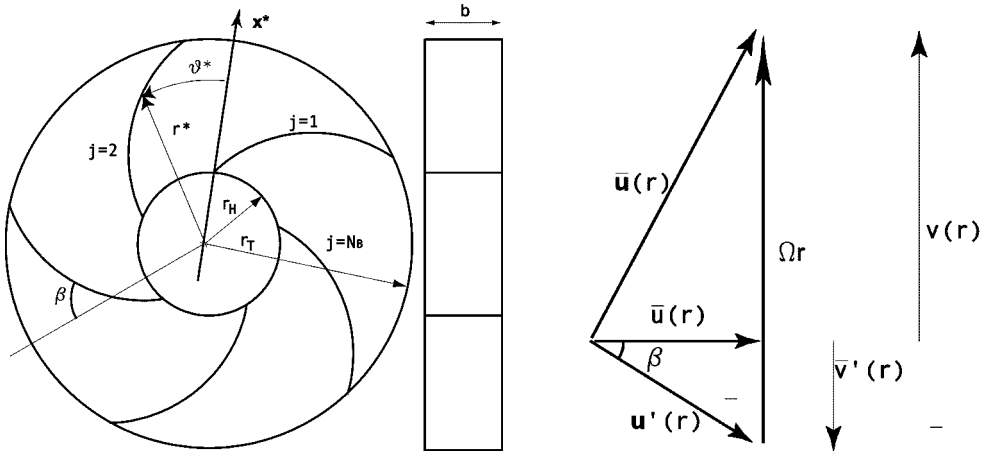

Figure 9. Schematic of the radial impeller geometry (left) and flow velocity triangle (right).

We define again stationary cylindrical coordinates r, ϑ, z with center in O on the axis of the stator, rotating cylindrical coordinates r', ϑ', z' spinning at the rotor speed with center in the same point O, and rotating and whirling cylindrical coordinates r^*, ϑ^*, z^* fixed in the inducer and with center in O^* on its geometric axis. Then the equations of the blade surfaces are:

$$B = \ln\frac{r}{r_H} + \left(\vartheta - \vartheta_j\right)\cot\beta = 0$$

where $\vartheta_j = 2\pi\left(j-1\right)\big/N_B$ is the angular location of the j-th blade, with $j = 1,2,...,N_B$. Once more the flow velocities in the stationary and rotating frames are related by $\boldsymbol{u} = \boldsymbol{u}' + \boldsymbol{\Omega}\times\boldsymbol{r}$ and, to the first order in the eccentricity (Fig. 3):

$$r^* = r - \varepsilon\cos\left(\vartheta - \omega t\right) = r' - \varepsilon\cos\left(\vartheta' - \omega' t\right)$$

$$\vartheta^* = \vartheta - \Omega t + \frac{\varepsilon}{r}\sin\left(\vartheta - \omega t\right) = \vartheta' + \frac{\varepsilon}{r}\sin\left(\vartheta' - \omega' t\right)$$

$$z^* = z' = z\ .$$

where $\omega' = \omega - \Omega$.

The perturbation velocity $\tilde{\boldsymbol{u}}$ generated by the blade motion is irrotational ($\tilde{\boldsymbol{u}} = \nabla\varphi$) because the flow originates from a uniform stream. Therefore, in the rotating frame the flow velocity is $\boldsymbol{u}' = \boldsymbol{u} - \boldsymbol{\Omega}\times\boldsymbol{r}$ and the Bernoulli's equation writes:

$$\int\frac{\partial'\boldsymbol{u}'}{\partial t}\cdot d\boldsymbol{x} + \frac{1}{2}\boldsymbol{u}'\cdot\boldsymbol{u}' - \frac{1}{2}\Omega^2\boldsymbol{r}\cdot\boldsymbol{r} + \frac{p}{\rho_L} = C\left(t\right)$$

where $C\left(t\right)$ is the unsteady Bernoulli's constant. Hence the linearized governing equations for the flow perturbations (tildes) at any given point in the rotating frame are:

$$\nabla^2\tilde{\varphi} = 0 \qquad \text{and} \qquad \frac{\partial'\tilde{\varphi}}{\partial t} + \bar{\boldsymbol{u}}'\cdot\nabla\tilde{\varphi} + \frac{\tilde{p}}{\rho_L} = 0$$

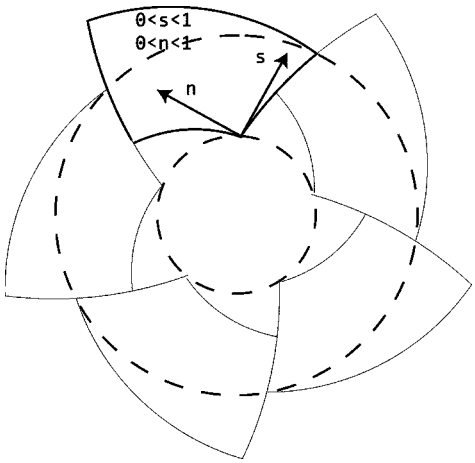

Figure 10. Schematic of the logarithmic-spiral coordinates.

Here the flow velocity must satisfy the kinematic conditions $Db/Dt = 0$ on the hub, blade and casing surfaces of equations $b(\boldsymbol{x},t) = 0$ in the relevant coordinates. In addition, the total pressure is assumed constant on the inlet and outlet sections of the inducer.

In order to simplify the derivation of the solution, let us introduce orthogonal spiral coordinates n, s (Campos and Gil, 1995; Visser, 1999) as shown in Figure 10, with:

$$n = \frac{N_B}{2\pi}\left(\vartheta - \vartheta_j\right) + \frac{N_B}{2\pi}\ln\left(\frac{r}{r_H}\right)\tan\beta$$

$$n = -\frac{\sin\beta\cos\beta}{\ln\left(r_T/r_H\right)}\left(\vartheta - \vartheta_j\right) + \frac{\ln\left(r/r_H\right)}{\ln\left(r_T/r_H\right)}\cos^2\beta$$

For convenience, n and s are normalized to map a channel into a rectangle $(0,1)\times(0,1)$. Rotating and body-fixed orthogonal spiral coordinates n', s' and n^*, s^* are similarly defined in terms of r', ϑ' and r^*, ϑ^*. The third dimension z is easily added. Then, the equations of the inlet, blade pressure side, blade suction side and outlet surfaces are:

$$B = s^* = 0\,.$$

$$B = n^* = 0\,.$$

$$B = n^* - 1 + \delta = 0\,.$$

$$B = s^* - 1 = 0\,.$$

where $\delta = \delta(t)$.

From the continuity equation for the layer $\rho_C\delta \equiv \text{constant}$, the definition of $a_C^2 = dp/d\rho_C$ and the Bernoulli's equation $\tilde{p}/\rho_L \cong -\partial\tilde{\varphi}/\partial t$ it follows that:

$$\frac{d\delta}{dt} = \frac{\rho_L\delta}{\rho_C a_C^2}\frac{\partial^2\tilde{\varphi}}{\partial t^2}$$

With these results, and expressing $\nabla^2\tilde{\varphi}=0$ and $\partial B/\partial t+\bar{\boldsymbol{u}}'\cdot\nabla B=0$ in the rotating helical coordinates $r', n',' s'$:

$$\nabla'^2\tilde{\varphi}=\frac{\cos^2\beta}{\ln^2\left(r_T/r_H\right)}\frac{\partial^2\tilde{\varphi}}{\partial s'^2}+\frac{N_B^2}{4\pi^2\cos^2\beta}\frac{\partial^2\tilde{\varphi}}{\partial n'^2}=0$$

and the linearized boundary conditions are found to be:

$$\frac{\partial\tilde{\varphi}}{\partial t}=0 \qquad \text{on} \qquad s'=1 \quad \text{and} \quad s'=0$$

$$\frac{\partial\tilde{\varphi}}{\partial n'}=\varepsilon\frac{2\pi}{N_B}\left[\omega' r_H\left(\frac{r_T}{r_H}\right)^{s'}\cos^2\beta\sin\beta\left(\frac{\cos\Theta'}{\sin\beta}+\frac{\sin\Theta'}{\cos\beta}\right)+\right.$$

$$\left.+\left(\frac{r_T}{r_H}\right)^{1-s'}\bar{u}_T\sin\Theta'\right] \qquad \text{on} \qquad n'=0$$

$$\frac{N_B}{2\pi}K_E\frac{\partial^2\tilde{\varphi}}{\partial t^2}+\frac{N_B}{2\pi r_H^2\left(r_T/r_H\right)^{2s'}\cos^2\beta}\exp\left(-\frac{4\pi}{N_B}\sin\beta\cos\beta\right)\frac{\partial\tilde{\varphi}}{\partial n'}=$$

$$=\varepsilon\omega'\frac{\sin\beta}{r_H\left(r_T/r_H\right)^{s'}}\exp\left(-\frac{2\pi}{N_B}\sin\beta\cos\beta\right)\left(\frac{\cos\Theta'}{\sin\beta}+\frac{\sin\Theta'}{\cos\beta}\right)+$$

$$+\varepsilon\frac{\bar{u}_T}{r_H^2}\left(\frac{r_T}{r_H}\right)^{1-3s'}\exp\left(-\frac{6\pi}{N_B}\sin\beta\cos\beta\right)\frac{\sin\Theta'}{\cos^2\beta} \qquad \text{on} \quad n'=1$$

Here:

$$\Theta'=\vartheta'-\omega' t=\vartheta_j+\frac{2\pi}{N_B}n'\cos^2\beta-s'\ln\left(\frac{r_T}{r_H}\right)\tan\beta-\omega' t$$

and:

$$K_E=\frac{4\pi^2\rho_L\delta}{N_B^2\rho_C a_C^2}\cos^2\beta$$

is a parameter describing the dynamic behavior of the cavitating layer and the extent of cavitation.

With the above boundary conditions the Laplace equation for $\tilde{\varphi}=\mathrm{Re}\left\{\hat{\varphi}\right\}$ yields a well-posed boundary value problem for the complex velocity potential $\hat{\varphi}$. The separable solution in the blade channels is:

$$\hat{\varphi}=\sum_{m=1}^{+\infty}\left\{\left[c_1\cosh\left(n'\sqrt{\nu_m^2}\right)+c_2\sinh\left(n'\sqrt{\nu_m^2}\right)\right]\sin\left(m\pi s'\right)\right\}e^{-i\omega' t}$$

with eigenvalues:

$$\sqrt{\nu_m^2}=i\frac{2m\pi^2\cos^2\beta}{N_B\ln\left(r_T/r_H\right)}$$

The instantaneous fluid force on the inducer is then:

$$\tilde{\boldsymbol{F}} = \int_{\text{blades}} \tilde{p}\left(\boldsymbol{r}'\big|_{\varepsilon\neq 0}, t\right) d\boldsymbol{S}$$

where, with second order error in the perturbations, the pressure:

$$\tilde{p} = -\rho_L \frac{\partial \tilde{\varphi}}{\partial t} - \rho_L \bar{\boldsymbol{u}}' \cdot \nabla \tilde{\varphi}$$

is evaluated for at the unperturbed position of the impeller ($\varepsilon = 0$). Because no hub is present, no buoyancy force acts on the displaced inducer due to the radial gradient of the mean pressure. The components of the instantaneous rotordynamic force are therefore obtained by integrating the projections of the elementary pressure forces along the axes of the whirling frame of center in O^* and unit vectors $\boldsymbol{e}_R, \boldsymbol{e}_T$, oriented as the eccentricity and its normal in the direction of the whirl motion. Finally, further integration over a period $2\pi/\omega'$ yields the time-averaged rotordynamic force $\boldsymbol{F}$ on the inducer.

The flow has then been determined in terms of the material properties of the two phases, the geometry of the inducer, the nature of the excitation, and the assigned quantities ϕ, δ, ρ_C, a_C.

5 Rotordynamic Forces on Whirling and Cavitating Radial Impellers

In centrifugal pumps, the measured rotordynamic fluid forces in the presence of cavitation are nearly equal to those for fully-wetted flows (Jery, 1987; Franz et al., 1989). Here the rotordynamic fluid forces predicted by the present model are compared with the data measured by Jery (1987) at Caltech on a five-bladed centrifugal pump with $r_T = 81$ mm, $r_H = 40$ mm, $\beta = 23°$, $b = 16$ mm, $\varepsilon = 0.126$ mm, without cavitation. The data refer to operation in water at room temperature, flow coefficient $\phi = 0.092$, rotational speed $\Omega = 1000$ rpm, and variable whirl speed. The results obtained by Franz (1989) for a cavitating radial impeller with a volute are also very similar.

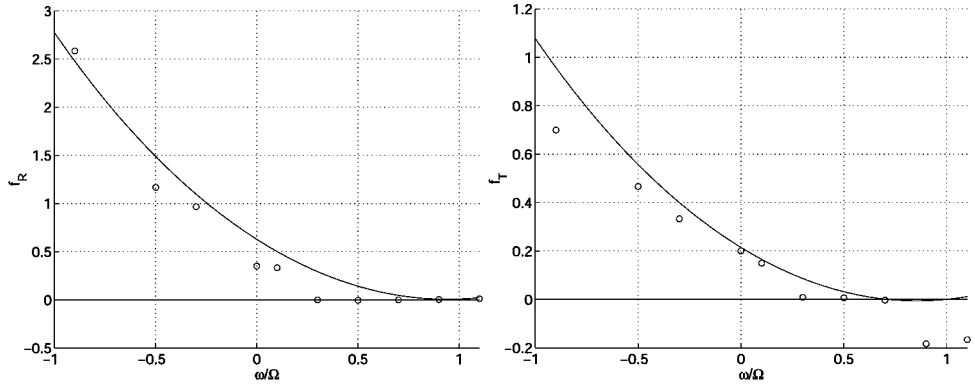

Figure 11. Comparison of the normalized radial (left) and tangential (right) rotordynamic forces, f_R and f_T, obtained from the present theory (continuous line) and the experimental results of Jery, 1987 (divided by six, circles) for a centrifugal impeller with $\Omega = 1000$ rpm, $N_B = 5$, $\phi = 0.060$, $\beta = 23°$, $r_T = 81$ mm, $b = 16$ mm, $r_H / r_T = 0.5$ and $\Omega^2 K_E = 2$.

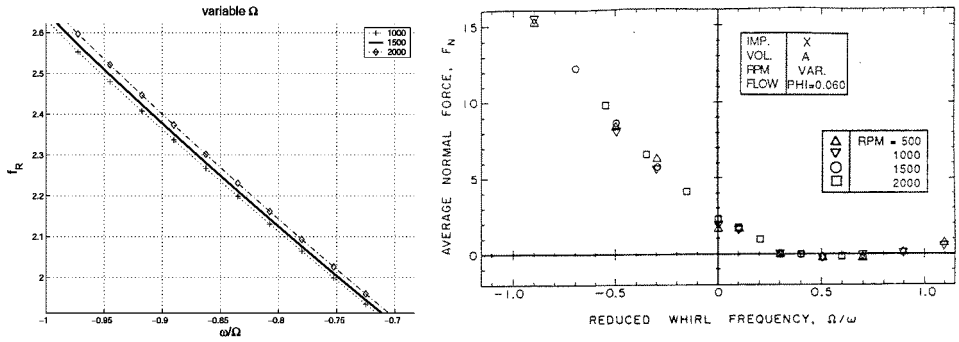

Figure 12. Comparison of the normalized radial rotordynamic force, f_R, obtained from the present theory (left) for $K_E = 2 \cdot 10^{-5}$ sec^2 and several rotational speeds Ω with the experimental results (right) of Jery, 1987, for a centrifugal impeller with $N_B = 5$, $\phi = 0.060$, $\beta = 23°$, $r_T = 81$ mm, $b = 16$ mm and $r_H / r_T = 0.5$.

The calculated rotordynamic forces shown in the figures have been nondimensionalized by $\pi\varepsilon\rho_L r_T^2 \Omega^2 b$. Comparison with the experimental results by Jery (1987) in Figure 11 shows that the calculated forces are about six times smaller than experimentally measured, but their familiar quadratic behavior with the whirl speed is well captured by the theoretical results and the vertex of the parabola is correctly located. The reasons for the observed discrepancy have not been identified with certainty, but they are likely to be mostly related to the approximate nature of the boundary conditions at the inlet and outlet sections of the impeller. In their present form these boundary conditions do not realistically account for the dynamic response of the flow in the impeller eye and diffuser (or volute). The inclusion of these effects would introduce significant additional contributions to the inertial reaction of the flow on the impeller, increasing the magnitude of the rotordynamic forces.

Clearly with present notations rotordynamic forces are destabilizing when the radial component is positive and, for the onset of asynchronous whirl, when the tangential component has the same sign as the whirl speed ω. Hence, with reference to Figure 11, the predicted radial force is generally destabilizing except near synchronous conditions ($\omega \cong \Omega$), while the tangential force would promote subsynchronous shaft motions in the range of whirl speeds $0 < \omega < 0.7$. Also notice that both components of the rotordynamic force are relatively small in the vicinity of $\omega / \Omega = 0.5$, corresponding to the familiar "whip conditions" of journal bearings (Newkirk and Taylor, 1925; Hori, 1959).

Present results for radial turbopumps are also radically different from those obtained for cavitating inducers. In this case both the experiments of Bhattacharyya et al. (1997) and our previous theoretical investigations based on the same approach used herein (d'Agostino, d'Auria and Brennen (1998), d'Agostino and Venturini (2002, 2003) showed a more complex dependence of the rotordynamic forces on the whirl speed. The spectral response of these forces as functions of the whirl frequency displayed a number of multiple peaks, which the theory indicated to be related with the occurrence of internal resonances of the cavitating flow in the blade channels under the excitation provided by the eccentric motion of the inducer. From the mathematical standpoint,

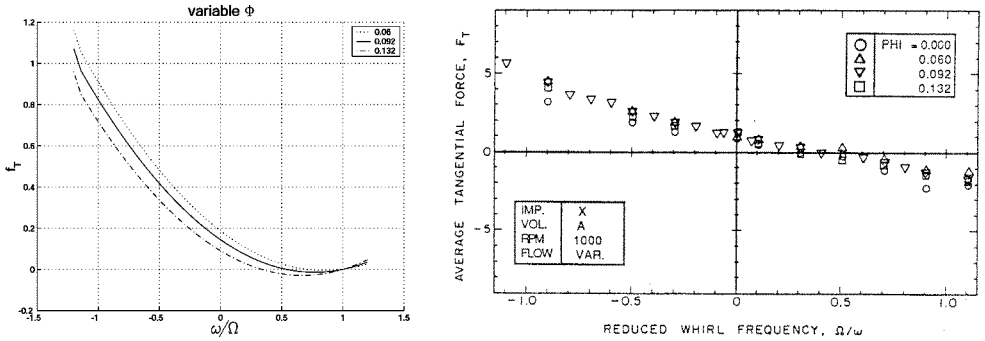

Figure 13. Comparison of the normalized tangential rotordynamic force, f_T, obtained from the present theory (left) for $\Omega^2 K_E = 2$ and several rotational speeds Ω with the experimental results (right) of Jery, 1987, for a centrifugal impeller with $N_B = 5$, $\phi = 0.060$, $\beta = 23°$, $r_T = 81$ mm, $b = 16$ mm and $r_H / r_T = 0.5$.

these resonances are the consequence of the (nearly) real nature of the flow eigenvalues, which leads to an infinite set of lowly-damped critical whirl speeds, symmetrically located above and below the rotational speed Ω (synchronous conditions). Physically, the peaks of the rotordynamic forces are due to the occurrence of standing pressure waves with frequency-dependent wavelength in the blade channels. Hence, at some specific excitation frequencies the wavelength of the resonant flow perturbations is an odd multiple of the blade channel revolution around the hub. In this case the pressure distribution acts in a strong and spatially coherent fashion on the inducer, leading to the intensification of the resulting forces.

Rotordynamic forces on radial impellers, on the other hand, do not peak at any whirl frequency. Mathematically, in this case the critical whirl speeds are (nearly) imaginary:

$$\omega'_m = \pm i\pi e^{-\frac{2\pi}{N_B}\sin\beta\cos\beta} \sqrt{\frac{2m}{K_E N_B r_H r_T \ln\left(r_T/r_H\right)} \tan\frac{2m\pi^2\cos^2\beta}{N_B \ln\left(r_T/r_H\right)}}$$

Physically, in radial impellers the presence of the blades prevents the formation of synchronous pressure waves with significant extension in the azimuthal direction, capable of reacting in a coherent fashion on the impeller.

Notice that the flow solution depends on the parameter K_E, whose relationship with the extent of cavitation has already been investigated in our earlier work (d'Agostino and Venturini, 2002) with the help of a quasi-homogeneous isenthalpic cavitation model with thermal effects (Rapposelli and d'Agostino, 2001). However, as mentioned earlier, rotordynamic forces are only weakly dependent on the extent of cavitation and the value of K_E.

The capability of the model of qualitatively capturing the main phenomena controlling the development of rotordynamic fluid forces in whirling centrifugal impellers is confirmed by Figures 12 and 13, which illustrate the sensitivity of the solution to changes of the rotational speed Ω and flow coefficient ϕ. In both cases the predicted impact of these parameters is small, consistently with typical experimental results from Jery (1987) shown in the right diagram of the figure. The forces in Figure 12 have been calculated with fixed K_E and therefore variable $E = \Omega^2 K_E$. With variable Ω and constant K_E the computed curves overlap, showing that K_E

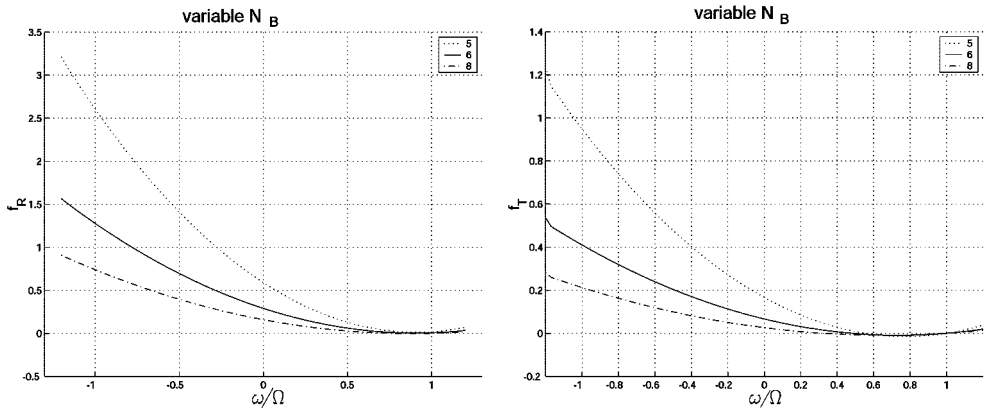

Figure 14. Normalized radial (left) and tangential (right) rotordynamic forces, f_R and f_T, predicted by the present theory as functions of the whirl ratio ω/Ω for a centrifugal impeller with variable number of blades $N_B = 5$ (dotted line), 6 (solid line) and 8 (dash-dotted line), $\Omega = 1000$ rpm, $\phi = 0.092$, $\beta = 23°$, $r_T = 81$ mm, $r_H = 40$ mm, $b = 16$ mm and $\Omega^2 K_E = 1$.

is a well-suited similarity parameter for cavitation effects. Besides, the curves computed for constant Ω and variable K_E (not shown here) almost overlap, confirming that in radial impellers the rotordynamic forces are practically insensitive to cavitation, in accordance with the experimental data by Franz et al. 1989.

Figure 13 shows the negligible influence of the flow coefficient ϕ on the rotordynamic forces. Also this finding agrees well with the experimental data. However, it should be emphasized that different values of Ω and ϕ correspond to very different rotordynamic forces in axial inducers, and that our approach to cavitation modeling correctly reflect this aspect (d'Agostino and Venturini, 2002; Venturini, 2003).

The present theory can also be used to investigate the dependence of rotordynamic whirl forces on the impeller geometry. Specifically, Figures 14, 15 and 16 illustrate the predicted effects of the number of blades, N_B, the blade angle, β, and the hub-to-tip radius ratio, r_H/r_T. As expected, the magnitude of rotordynamic forces decreases as the number of blades increases, but their stabilizing/destabilizing nature is not significantly affected (Figure 14). In this respect it is worth noting that the accuracy of the model increases with N_B because the spiral coordinate system more closely approximates the actual geometry of the impeller when the blade channels are narrower.

Figure 15 shows that both the radial and tangential components of the rotordynamic force decrease at lower blade angles. At higher values of $\beta = 40°$ the radial force is destabilizing only for negative whirl, and the tangential force undergoes two zero crossings, being potentially destabilizing only for supersynchronous whirl ($\omega/\Omega > 1$), where, however, the radial force is not capable of sustaining the eccentricity of the impeller.

Finally, Figure 16 shows that rotordynamic forces and their stabilizing/destabilizing properties are relatively insensitive to the hub-to-tip radius ratio, at least in the range of values meaningful for radial impellers.

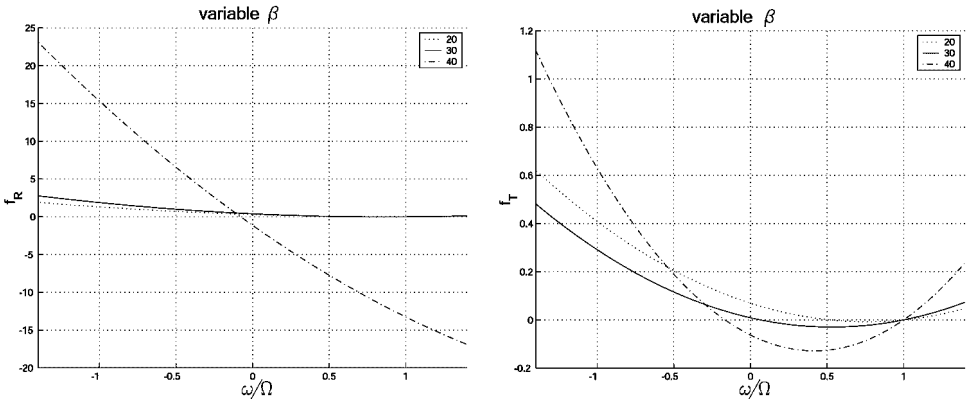

Figure 15. Normalized radial (left) and tangential (right) rotordynamic forces, f_R and f_T, predicted by the present theory as functions of the whirl ratio ω/Ω for a centrifugal impeller with variable blade angle $\beta = 20°$ (dotted line), 30° (solid line) and 40° (dash-dotted line), $N_B = 7$, $\Omega = 1000$ rpm, $\phi = 0.092$, $r_T = 81$ mm, $r_H = 40$ mm, $b = 16$ mm and $\Omega^2 K_E = 1$.

6 Limitations

We now briefly examine the restrictions imposed to the present theory by the various simplifying approximations that have been made. Specifically we shall discuss the limitations due to the assumption of thin-layer cavitation, to the neglect of Coriolis forces, to the applicability of the formulation in orthogonal helical coordinates to the analysis of cavitating impellers, and to the use of the linear perturbation approach in deriving the solution.

The assumption of thin-layer cavitation implies that the thickness of the cavitating region is significantly smaller than the blade channel width and that its properties can be approximated as constant over the entire length of the blades for the purpose of evaluating the rotordynamic forces. Although clearly none of these conditions is rigorously met in cavitating impellers, comparison with earlier results obtained by d'Agostino and his collaborators (1997, 1998) for uniformly distributed bubbly cavitation shows that the predicted values of the rotordynamic forces are remarkably independent on the precise geometry of flow cavitation.

The neglect of Coriolis forces implies that $\Omega_F << \Omega$, a condition that is approximately satisfied in moderately loaded impellers.

For the formulation in orthogonal helical coordinates to be valid the geometric length of the blades should be comparable to their actual overlap, which is rarely the case in low blade angle inducers. Formally, this is probably one of the most stringent limitations of the present analysis and can only be partially circumvented by artificially introducing an empirical "effective length" of the blade channels.

Finally, the perturbation approach simply requires that $\varepsilon << r_T$, a condition that can safely be assumed in the analysis of whirl instabilities of cavitating turbomachines.

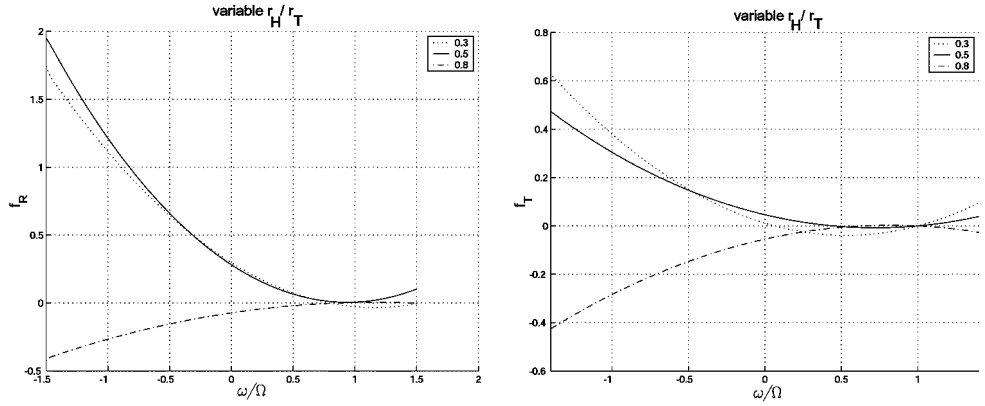

Figure 16. Normalized radial (left) and tangential (right) rotordynamic forces, f_R and f_T, predicted by the present theory as functions of the whirl ratio ω/Ω for a centrifugal impeller with variable hub-to-tip radius ratio $r_H/r_T = 0.3$ (dotted line), 0.5 (solid line) and 0.8 (dash-dotted line), $N_B = 7$, $\Omega = 1000$ rpm, $\phi = 0.092$, $\beta = 23°$, $r_T = 81$ mm, $b = 16$ mm and $\Omega^2 K_E = 1$.

7 Summary and Conclusions

This investigation reveals a number of important flow phenomena occurring in whirling and cavitating helical inducers. The results clearly indicate that blade cavitation drastically modifies the rotordynamic forces exerted on the inducer by the surrounding fluid. The dynamic response of the cavitating flow to the periodic excitation imposed by the whirl motion generates multiple subsynchronous and supersynchronous flow resonances in the blade channels, interfering with the more regular spectral behavior of the rotordynamic fluid forces, typical of noncavitating operation. The extent of cavitation has a major impact in locating the critical speeds and determining the intensity of flow-induced rotordynamic forces. At higher levels of cavitation the amplitudes of the flow resonances decrease, and their frequencies approach the rotational speed of the inducer (synchronous conditions).

On the other hand, the present theory predicts that blade cavitation does not appreciably modify the rotordynamic fluid forces on whirling and centrifugal impellers, in accordance with the experimental evidence and in striking contrast with the observed behavior of axial inducers. Comparison with the results of the analysis of cavitating inducers confirms that the contribution of cavitation to the rotordynamic whirl forces is only significant when the standing pressure waves excited in the blade channels by the impeller motion are capable of exerting synchronous and coherent actions on the rotor. For this to happen:

- the blade channels must be long enough in the azimuthal direction for the pressure wave to become at least partly coherent with the channel rotation around the axis: only in this case the resulting forces do not average out and generate appreciable fluid reactions on the rotor;
- possibly the cavitating flow in the blade channels must become resonant, in order to maximize the amplitude of the pressure fluctuations.

The first condition can never be satisfied in radial impellers due to the limited azimuthal extension of the blade channels. This geometric limitation is the essential reason for the different behavior rotordynamic whirl forces in cavitating radial and axial impellers. Besides, according to the present theory, no resonance phenomena can occur in whirling and cavitating centrifugal impellers because the natural frequencies of the flow are essentially imaginary.

In spite of its approximate nature, the present theory correctly captures the main observed features and different behavior of the rotordynamic forces in axial inducers and radial impellers. There is therefore reason to believe that it contributes some useful fundamental insight into the complex physical phenomena responsible for the onset and sustain of free-whirl instabilities in cavitating turbopumps.

8 Acknowledgements

The present work has been partially supported by the Agenzia Spaziale Italiana under a 1999 grant for fundamental research. The author would like to acknowledge the help of Dr. Marco Venturini-Autieri, and express his gratitude to Prof. Mariano Andrenucci, Director of Alta S.p.A., Ospedaletto (Pisa), Italy, and to Prof. Renzo Lazzeretti of the Dipartimento di Ingegneria Aerospaziale, Università degli Studi di Pisa, Pisa, Italy, for their constant and friendly encouragement.

9 Nomenclature

a	sound speed
A	cross-sectional flow area
b	axial length of the radial impeller
B	boundary equation
c	specific heats, constant
$\boldsymbol{e}$	unit vector
f	nondimensional force
F	force
i	imaginary unit
I	modified Bessel function of the first kind, integral
j	blade index
J	Bessel function of the first kind
k	hub excitation mode index
K	modified Bessel function of the second kind
K_C, K_E	cavitating layer parameters
L	axial length of the inducer
L^*	blade axial length
l	blade excitation mode index
m	streamwise mode index
n	blade-to-blade helical/spiral coordinate
N	blade-to-blade mode function
N_B	number of blades
N_R	number of blade revolutions

O , O^*	origin of coordinate systems
p	pressure
p_t	total or stagnation pressure
P	blade axial pitch
P^*	blade-to-blade distance
$\dot{Q}$	volume flow rate
r	radial coordinate, radius
$\boldsymbol{r}$	radial vector
R	radial mode function, cavity radius
s	streamwise helical/spiral coordinate
S	surface, streamwise mode function
t	time
T	temperature, aspect ratio
u	radial velocity component
$\boldsymbol{u}$	velocity vector
v	azimuthal velocity component
w	axial velocity component
x	abscissa
y	ordinate
Y	Bessel function of the second kind
z	axial coordinate
α	void fraction
β	blade angle
δ	cavitation layer thickness
δ_T	thermal boundary layer thickness
ε	whirl eccentricity
ζ	nondimensional damping coefficient
ϑ	azimuthal angle
λ	radial eigenvalue
μ	streamwise eigenvalue
ν	blade-to-blade eigenvalue
ρ	density
σ	cavitation number
φ	velocity potential
ϕ	flow coefficient
ω	whirl angular velocity
Ω	inducer rotational speed

Subscripts and Superscripts

B	blade
C	cavitation
F	mean flow
H	hub
L	liquid

M	mean
R	radial
T	tangential, blade tip
V	vapor
$\overline{q}$	unperturbed value of q
$\tilde{q}$	perturbation value of q
$\hat{q}$	complex representation of $\tilde{q}$
q'	derivative, value of q in the rotating frame
q^*	value of q in the inducer-fixed frame
1	inducer inlet
2	inducer outlet

Bibliography

Adkins, D.R. and Brennen, C.E., 1988, "Analysis of Hydrodynamic Radial Forces on Centrifugal Pump Impeller", *ASME Journal of Fluids Engineering*, Vol. 110, pp. 20-28.

Alford J.S., 1958, "Protecting Turbomachinery from Self-Excited Rotor Whirl", *ASME J. Eng. Power*, Vol. 87, pp. 333-334.

Arndt, N., and Franz, R., 1986, "Observation of Hydrodynamic Forces on Several Inducers Including the SSME LPOTP", *Report No. E249.3*, Division of Engineering and Applied Sciences, California Institute of Technology, Pasadena, California.

Arndt N. et al., 1989, "Rotor-Stator Interaction in a Diffuser Pump", *ASME J. Turbomachinery*, Vol. 111, pp. 213-221.

Arndt N. et al., 1990, "Experimental Investigation of Rotor-Stator Interaction in a Centrifugal Pump with Several Vaned Diffusers", *ASME J. Turbomachinery*, Vol. 112, pp. 98-108.

Baskharone, E.A., 1999, "Swirl Brake Effect on the Rotordynamic Stability of a Shrouded Impeller", *ASME Journal of Turbomachinery*, Vol. 121, pp. 127-133.

Bhattacharyya, A., 1994, "Internal Flows and Force Matrices in Axial Flow Inducers", *Ph.D. Thesis*, Division of Engineering and Applied Science, California Institute of Technology, Pasadena California.

Bhattacharyya, A., Acosta, A.J., Brennen, C.E., and Caughey, T.K., 1997, "Rotordynamic Forces in Cavitating Inducers", *ASME Journal of Fluids Engineering*, Vol. 199, No. 4, pp. 768-774, ISSN 0098-2202.

Brennen, C. E., 1994, "Hydrodynamics of Pumps", *Concepts ETI, Inc.,* P.O. Box 643, Norwich, Vermont 05055, USA, ISBN 0-933283-07-5, and *Oxford University Press*, Walton St., Oxford OX2 6DP, England, ISBN 0-19-856442-2.

Brennen, C., E., 1995, "Cavitation and Bubble Dynamics", *Oxford University Press*.

Campos L.M.B.C. and Gil P.J.S., 1995, "On Spiral Coordinates with Application to Wave Propagation", *J. Fluid Mechanics*, Vol. 301, pp. 153-173.

Chamieh D.S. et al., 1985, "Experimental Measurements of Hydrodynamic Radial Forces and Stiffness Matrices for a Centrifugal Pump Impeller", *ASME Journal of Fluids Engineering*, Vol. 107, pp. 307-315.

d'Agostino L. and d'Auria F., 1997, "Three-Dimensional Analysis of Rotordynamic Forces on Whirling and Cavitating Inducers", *ASME Paper FEDSM97-3335, 1997 ASME Fluids Engineering Division Summer Meeting*, Vancouver, British Columbia, Canada, June 22-26.

d'Agostino L., d'Auria F. and Brennen C.E., 1998, "A Three-Dimensional Analysis of Rotordynamic Forces on Whirling and Cavitating Helical Inducers", *ASME Journal of Fluids Engineering*, Vol. 120, pp. 698-704.

d'Agostino L. and Venturini-Autieri M.R., 2002, "Three-Dimensional Analysis of Rotordynamic Fluid Forces on Whirling and Cavitating Finite-Length Inducers", *9th Int. Symp. on Transport Phenomena and Dynamics of Rotating Machinery (ISROMAC-9),* Honolulu, HI, USA, February 10-14.

d'Agostino L. and Venturini-Autieri M.R., 2003, "Rotordynamic Fluid Forces on Whirling and Cavitating Radial Impellers", *CAV 2003, 5th International Symposium on Cavitation*, November 1-4, Osaka, Japan.

d'Auria, F., d'Agostino, L., Brennen, C.E., 1995, "Bubble Dynamics Effects on the Rotordynamics Forces in Cavitating Inducers", *1995 ASME Cavitation and Multiphase Flow Forum*, Hilton Head Island, South Carolina, USA, FED Vol. 201, pp. 47-54.

Franz R. et al., 1989, "The Rotordynamic Forces on a Centrifugal Pump Impeller in the Presence of Cavitation", *ASME-F.E.D. 81*, 205-212.

Hiwata A. and Tsujimoto Y., 2002, "Theoretical Analysis of Fluid Forces on and Open-Type Centrifugal Impeller in Whirling Motion", *ASME J. Fluids Eng*., Vol. 124, pp. 342-347.

Hori Y., 1959, "The Theory of Oil Whip", *ASME J. Appl. Mech*., Vol. 26, pp. 189-198.

Jery, B., Acosta A. J., and Caughey, T. K.,, 1985, "Forces on Centrifugal Pump Impellers", *Proc. 2nd Int. Pump Symp*., Houston, Texas, USA, April 29-May 2.

Jery, B. 1987, "Experimental Study of Unsteady Hydrodynamic Force Matrices on Whirling Centrifugal Pump Impellers", *Report No. E200.22*, Division of Engineering and Applied Sciences, California Institute of Technology, Pasadena, California, USA.

Lebedev, N.N., 1965, "Special Functions and Their Applications", *Prentice Hall*.

Martinez-Sanchez M., Jaroux B., Song S.J. and Yoo S., 1995, "Measurement of Turbine Blade-Tip Rotordynamic Excitation Forces", *ASME J. Turbomachinery*, Vol. 117, pp. 384-393.

Martinez-Sanchez M. and Song S.J., 1997a, "Rotordynamic Forces Due to Turbine Tip Leakage-Part I: Blade Scale Effects", *ASME J. Turbomachinery*, Vol. 119, pp. 695-703.

Martinez-Sanchez M. and Song S.J., 1997b, "Rotordynamic Forces Due to Turbine Tip Leakage-Part II: Radius Scale Effects and Experimental Verification", *ASME J. Turbomachinery*, Vol.119, pp. 704-717.

Newkirk B.L. and Taylor H.D., 1925, "Shaft Whipping due to Oil Action in Journal Bearing", *General Electric Review*, August 1925, pp. 559-568.

Ohasi H. and Shoji H., 1987, "Lateral Fluid Forces on Whirling Centrifugal Impeller (2nd Report: Experiment in Vaneless Diffuser)", *ASME Journal of Fluids Engineering*, Vol. 109, pp. 100-106.

Rapposelli, E., and d'Agostino, L., 2001, "A Modified Isenthalpic Model of Cavitation in Plane Journal Bearings", *CAV2001, International Symposim on Cavitation*, Pasadena, California USA, June 20-23.

Rosenmann, W., 1965, "Experimental Investigations of Hydrodynamically Induced Shaft Forces with a Three Bladed Inducer", *Proc. ASME Symp. on Cavitation in Fluid Machinery*, pp. 172-195.

Shoji, H. and Ohashi, H., 1987, "Lateral Fluid Forces on Whirling Centrifugal Impeller (1st Report: Theory)", *ASME Journal of Fluids Engineering*, Vol. 109, pp. 94-99.

Thomas J.H., 1958, "Instabile Eigenschwingungen von Turbinenlaufern Angefacht durch die Spaltstroemung in Stopfubuchsen und Bechauchflug (Unstable Natural Vibrations of Turbine Rotors Induced by Clearance Flows in Glands and Bladings)", *Bull. De. L.A.I.M.,* Vol. 71, pp. 1039-1063.

Tsujimoto, Y, Yoshida, Y., Ohashi, H., Teramoto, N. and Ishizaki, S., 1997, "Fluid Force Moment on a Centrifugal Impeller Shroud in Precessing Motion", *ASME Journal of Fluids Engineering*, Vol. 119, pp. 366-371.

Uy, R.V., and Brennen, C.E., 1999, "Experimental Measurements of Rotordynamic Forces Caused by Front Shroud Pump Leakage", *ASME Journal of Fluids Engineering*, Vol. 121, pp. 633-637.

Venturini-Autieri M.R., 2003, "Analisi delle Forze Rotodinamiche in Turbomacchine Cavitanti", *Tesi di Laurea, Dipartimento di Ingegneria Aerospaziale*, Università di Pisa, Pisa, Italy.

Visser F.C., 1999, “On the Asymptotic Solution of the Poisson Equation Describing the Two-Dimensional Incompressible Inviscid Flow in a Rotating Centrifugal Impeller”, *Zeitschrift für Angewandte Mathematik und Mechanik*, Vol. 79 (5), pp. 353-356.